The *Drosophila* inner-membrane protein PMI controls crista biogenesis and mitochondrial diameter

Marc Macchi[1], Najla El Fissi[1], Roberta Tufi[2], Mélanie Bentobji[1], Jean-Charles Liévens[3], L. Miguel Martins[2], Julien Royet[1,*] and Thomas Rival[1,*]

[1]Aix-Marseille Université, CNRS, Institut de Biologie du Développement de Marseille-Luminy, UMR 7288, F-13288 Marseille, France
[2]MRC Toxicology Unit, Hodgkin Building, PO Box 138, University of Leicester, Lancaster Road, Leicester LE1 9HN, UK
[3]Aix-Marseille Université, CNRS, Centre de Recherche en Neurobiologie et Neurophysiologie de Marseille, UMR 7286, Boulevard Pierre Dramard, F-13344 Marseille, Cedex 15, France

*Authors for correspondence (thomas.rival@univ-amu.fr; julien.royet@univ-amu.fr)

Accepted 3 December 2012
Journal of Cell Science 126, 814–824

doi: 10.1242/jcs.115675

Summary

Cristae are mitochondrial inner-membrane structures that concentrate respiratory chain complexes and hence regulate ATP production. Mechanisms controlling crista morphogenesis are poorly understood and few crista determinants have been identified. Among them are the Mitofilins that are required to establish crista junctions and ATP-synthase subunits that bend the membrane at the tips of the cristae. We report here the phenotypic consequences associated with the *in vivo* inactivation of the inner-membrane protein Pantagruelian Mitochondrion I (PMI) both at the scale of the whole organism, and at the level of mitochondrial ultrastructure and function. We show that flies in which *PMI* is genetically inactivated experience synaptic defects and have a reduced life span. Electron microscopy analysis of the inner-membrane morphology demonstrates that loss of *PMI* function increases the average length of mitochondrial cristae in embryonic cells. This phenotype is exacerbated in adult neurons in which cristae form a dense tangle of elongated membranes. Conversely, we show that PMI overexpression is sufficient to reduce crista length *in vivo*. Finally, these crista defects are associated with impaired respiratory chain activity and increases in the level of reactive oxygen species. Since PMI and its human orthologue TMEM11 are regulators of mitochondrial morphology, our data suggest that, by controlling crista length, PMI influences mitochondrial diameter and tubular shape.

Key words: Cristae, *Drosophila*, Mitochondrial morphogenesis, Oxidative metabolism

Introduction

Mitochondria are present in all eukaryotic cells where they play crucial functions including energy supply, apoptosis induction and calcium buffering (Nunnari and Suomalainen, 2012). Although involved in processes common to all cells, mitochondria are strikingly polymorphic organelles whose shape, length and diameter vary between cell types. Mitochondrial architecture is highly influenced by physiological and pathological conditions, highlighting the functional links between mitochondrial morphology and activity (Dürr et al., 2006; Detmer and Chan, 2007; Suen et al., 2008; Mitra et al., 2009; Tondera et al., 2009; Mitra et al., 2012; Nunnari and Suomalainen, 2012). If it is well established that mitochondria morphogenesis is supported by fusion and fission events regulated by dynamin-related GTPases (Mitofusin and DRP1) (Okamoto and Shaw, 2005; Westermann, 2010), the mechanisms by which mitochondria adopt their tubular shape, and regulate their diameter remain largely unknown. Recent evidence indicates that inner-membrane structures and their associated proteins are part of these processes (Dimmer et al., 2005; Okamoto and Shaw, 2005; Rabl et al., 2009; Velours et al., 2009; Zick et al., 2009; Head et al., 2011).

Mitochondria inner membranes are compartmentalized into domains such as inner-membrane boundaries, crista junctions and crista tubules that, by expressing specific proteins, support specific function (Frey and Mannella, 2000; Mannella, 2006a; Zick et al., 2009). Inner-membrane boundaries are contact sites between the inner and outer membranes that are maintained through physical links tethering the inner-membrane TIM complex to its outer-membrane counterpart, TOM (Vogel et al., 2006; Wurm and Jakobs, 2006). Cristae are invaginations that appear as straight and parallel tubular structures evenly distributed along the mitochondrial length (Mannella, 2006b; Zick et al., 2009). The opening of cristae onto the inter-membrane space, referred to as cristae junctions, consist of narrow tubules, which create a cristae-specific molecular environment by preventing the diffusion of membrane and soluble molecules (Frey and Mannella, 2000; Zick et al., 2009). Few molecular determinants of crista morphogenesis have been characterized in details. One of them, Mitofilin, assembles into the MINOS/MitOS/MICOS complex to support the formation of crista junctions (John et al., 2005; Xie et al., 2007; Rabl et al., 2009; Harner et al., 2011; Hoppins et al., 2011; von der Malsburg et al., 2011). OPA1, originally identified as a key effector of inner-membrane fusion, also controls the tightening of crista junctions (Olichon et al., 2003; Cipolat et al., 2006; Frezza et al., 2006; Meeusen et al., 2006). The non-catalytic subunits e and g of the F0F1 ATP-synthase (F0F1 e/g su) support the positive bending of crista tips (Strauss et al., 2008; Rabl et al., 2009). Finally, the regulation of inner-membrane component production

also impacts on crista morphogenesis. Consistently, mutations in the cardiolipin synthase tafazzin result in inner-membrane defects (Xu et al., 2006; Acehan et al., 2007), whereas loss of Prohibitin that affects inner-membrane phospholipid content inhibits crista growth (Osman et al., 2009b; Osman et al., 2009a).

Consistent with their role in crista organization, proteins coding for crista components indirectly control mitochondrial oxidative metabolism (John et al., 2005; Rabl et al., 2009), growth (John et al., 2005; von der Malsburg et al., 2011) and DNA content (Paumard et al., 2002), and their dysfunction has an impact at the organism level (Xu et al., 2006; Mun et al., 2010; Head et al., 2011). In human, abnormal inner-membrane organization is a common trait for many neuromuscular and metabolic diseases including Barth's syndrome (Acehan et al., 2007), Leigh's syndrome (Celotto et al., 2006), Alzheimer's disease (Baloyannis, 2006), amyotrophic lateral sclerosis (Chung and Suh, 2002), Wolfs Hirschhorn's syndrome (Hasegawa and van der Bliek, 2007; Dimmer et al., 2008) and polymyocitis (Zick et al., 2009).

In this manuscript, we described the consequences associated with an *in vivo* inactivation of *Drosophila* Pantagruelian Mitochondrion I (PMI), an inner-membrane protein that regulates mitochondrial morphogenesis (Rival et al., 2011). We show that loss of *PMI* function induces crista elongation and disorganization in *Drosophila* cells. We demonstrate that these inner-membrane abnormalities are associated with decreased oxidative metabolism and increased ROS production. We further show that at the organism scale, *PMI* mutation provokes synaptic defects and premature death of *Drosophila* adults. Altogether our results suggest that, by controlling crista biogenesis, PMI determines mitochondrial diameter explaining why *PMI* mutation also affects the overall tubular shape of mitochondria.

Results

PMI controls the morphogenesis of cristae

Several reports have highlighted the importance of inner-membrane proteins in mitochondrial crista morphogenesis (Paumard et al., 2002; Rabl et al., 2009; Harner et al., 2011; Hoppins et al., 2011; von der Malsburg et al., 2011). Having shown that PMI is an inner-membrane protein involved in the regulation of mitochondrial shape (Rival et al., 2011), we tested whether its inactivation would impact crista morphology in *Drosophila* embryos. In contrast to control mitochondria that form connected elongated tubules, mitochondria of *PMI* mutants form individualised spheres (Fig. 1A). Quantification of mitochondrial shape parameters on electron microscopy sections revealed that *PMI* mutant mitochondria contain significantly longer cristae than control mitochondria (Fig. 1C,D). This increase in length was correlated with an increase of the crista membrane length over outer membrane length ratio (*c.m./o.m.*; Fig. 1F). Conversely, we showed that PMI overexpression (*da-GAL4 UAS-PMI*) triggers a reduction of the average crista length and a decrease of the *c.m./o.m.* ratio (Fig. 1C,D,F). Despite this increased biogenesis, the overall morphology of the cristae was unaffected by *PMI* inactivation. As for wild type, *PMI* mutant cristae were quite straight and parallel (Fig. 1C4,G), although 10% of mitochondria display curved cristae suggesting that curvature is rather a consequence than a cause of increase length (Fig. 1C5). In addition, the diameter of PMI crista tubules was unaffected (Fig. 1H), and crista junctions were still present in *PMI* mutant mitochondria (Fig. 1I). We then compared *PMI* mitochondrial phenotype to that of *drp1* and *opa1* that are, respectively, effectors of mitochondrial fission and inner-membrane fusion. Consistent with the consequence of unbalanced fusion *drp1* mutant embryos display interconnected hanks of long tubular mitochondria (Fig. 1A). Conversely, the invalidation of the pro-fusion gene *opa1* results in the fragmentation of mitochondria into numerous small spherical entities (Fig. 1A). In contrast to *PMI* mutants, in *drp1* and *opa1* mutant mitochondria the crista length and *c.m./o.m.* ratio was normal (Fig. 1C,D,F). Similar results were obtained in adult brains in which *PMI* inactivation results in unique giant mitochondria in neurons instead of the thin tubules observed in the wild type (supplementary material Fig. S1A,B; Fig. S2A) (Rival et al., 2011). While mitochondria of wild-type neuron displayed straight, parallel and evenly spaced cristae (Fig. 2A,B), cristae from *PMI* mutant neurons appeared dramatically bent and longer than those in control mitochondria (Fig. 2A,B). At the mitochondrion periphery, *PMI* mutant inner-membrane invaginations often form concentric swirls that were never observed in controls (Fig. 2A,B). Although less pronounced, similar elongation and bending of crista membranes were also present in mitochondria from adult flight muscles (Fig. 3). To determine whether bending of *PMI* cristae was not a simple consequence of the overall increased size of mitochondria, we analysed *drp1* mutant mitochondria. As reported for *drp1* knockout mouse (Ishihara et al., 2009), *drp1* mutant mitochondria from adult fly neurons form giant masses, which are morphologically indistinguishable from those of *PMI* mitochondria (Rival et al., 2011). Although of same size and shape as *PMI* mitochondria, *drp1* mitochondria still contains straight and parallel cristae that are regularly distributed within the mitochondrial matrix as in wild-type cells (Fig. 1A). Taken together our results demonstrate that the inner-membrane protein PMI controls the elongation and the architecture of crista membranes.

By regulating the size of cristae, *PMI* influences mitochondrial diameter

In *PMI* mutant embryos, the average diameter of mitochondria is strongly increased compared to controls, a phenotype that is not observed in *drp1* or *opa1* mutants (Fig. 1B). To test whether the uncontrolled crista biogenesis seen in *PMI* mutants was related to increased mitochondrial diameter, we quantified these parameters in mutant embryos. These quantifications highlighted a direct correlation between crista length and mitochondrial diameter at this early developmental stage (Fig. 1E). Later, at the adult stage, *PMI* inactivation in adult brain neurons (Fig. 2A; supplementary material Fig. S1B; Fig. S2A) and in flight muscles (Fig. 3; supplementary material Fig. S3) was similarly associated with wider mitochondria. Conversely, PMI overexpression in adult flight myocytes was sufficient to trigger a dramatic reduction of mitochondrial diameter and length (*mef2-GAL4 UAS-PMI*; Fig. 3; supplementary material Fig. S3). This contrasted with *drp1* overexpression or knockdown of *opa1*, which reduced mitochondrial length without affecting the diameter (Fig. 3; supplementary material Fig. S3). Cristae from *PMI*-overexpressing myocytes appeared shorter and less packed than in wild-type mitochondria, consistent with a decreased in crista membrane biogenesis (Fig. 3). Again this contrasted with the wild-type cristae observed in *drp1*-overexpressing cells, or with the vacuolated and highly disorganised cristae from *opa1*

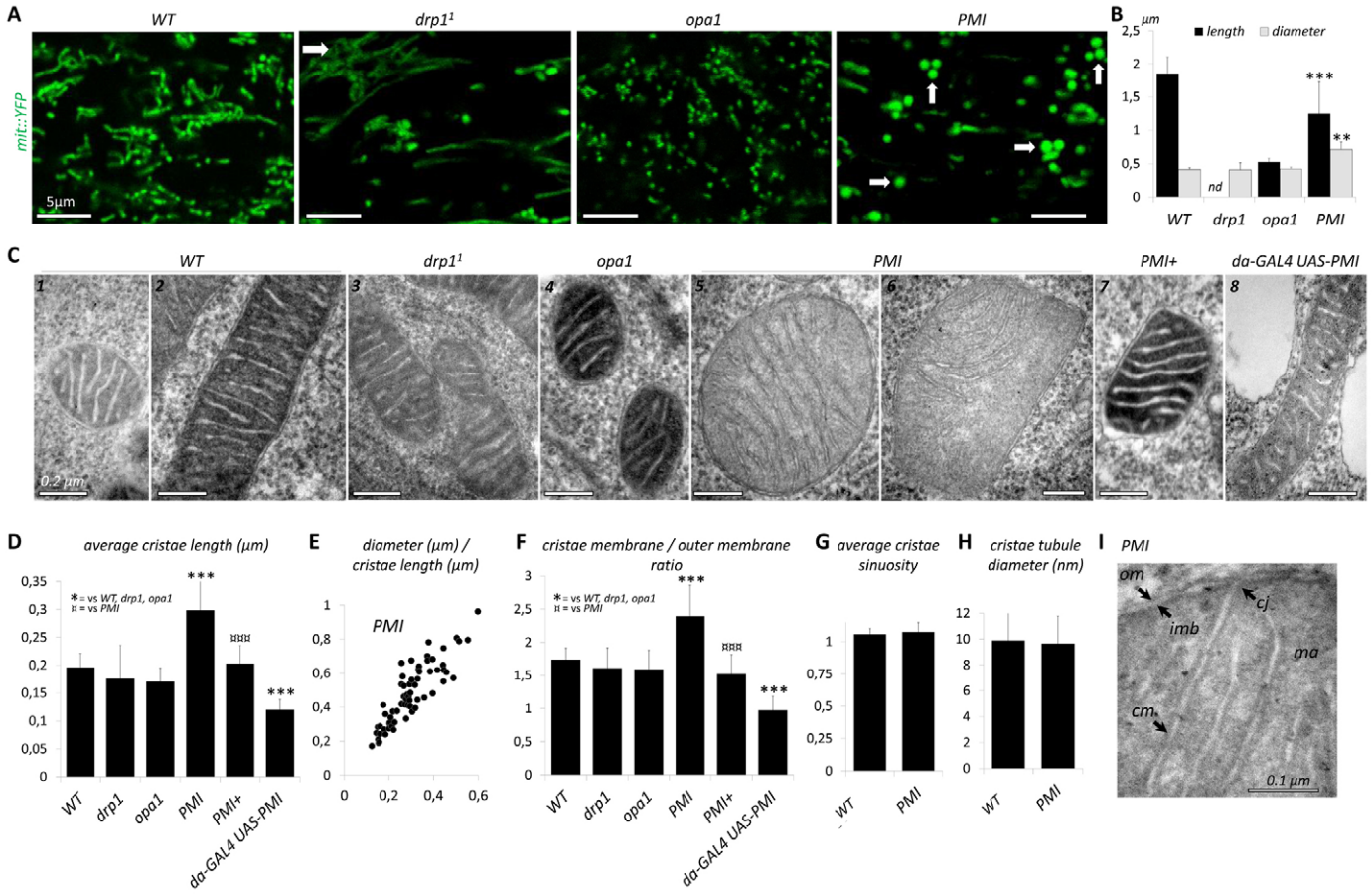

Fig. 1. PMI controls crista elongation. (**A**) Confocal sections of the ventral epidermis from wild-type, *drp1*, *opa1* and *PMI* mutant embryos at stage 13 expressing a *mit::YFP* fusion protein targeted to the mitochondrial matrix. *PMI* mutant mitochondria appear as large spheres (arrows) instead of forming the thin tubules normally seen in wild-type cells. *drp1* mutant mitochondria remain tubular but they are longer and form hanks of interconnected tubules (arrow). Conversely *opa1* mutant mitochondria are fragmented into numerous small spherical entities. (**B**) Average mitochondrial length (µm) and diameter (µm) in wild-type, *drp1*, *opa1* and *PMI* mutant embryos (ventral epidermis). The length of mitochondria is reduced in both *opa1* and *PMI* mutant compared to wild type. Whereas mitochondria from wild-type, *drp1* and *opa1* genotypes have similar diameter, *PMI* mutant mitochondria are significantly wider. A minimum of 60 mitochondria from at least three independent embryos were analysed for each condition. Length was not determined (nd) for *drp1* mutant because tubules form dense hanks, which make accurate measurements difficult. Statistical significance was analysed by one-way ANOVA (for diameter $P<0.0001$, for length $P<0.0001$) followed by Tukey HSD *post hoc* test (**$P<0.01$, ***$P<0.001$). (**C**) Transmission electron microscopy (TEM) pictures of mitochondria from stage 12–13 fly embryos (ventral epidermis). Wild-type (1, 2), *drp1* (3) and *opa1* (4) mitochondria contain evenly spaced, straight and parallel cristae. In contrast, *PMI* mutant mitochondria are wider and have elongated cristae (5, 6). Within a same embryo, cristae generally appear straight and parallel (5), although they can be bent (sinuosity >1.1) in 10% of the mitochondria (6). Consistently, those mitochondrial abnormalities are rescued in the control *PMI+* line (7) in which a genomic fragment containing the wild-type *PMI* sequence was inserted to restore PMI expression (see Materials and Method for details). (8) When PMI is overexpressed in a wild-type background the cristae are shorter and mitochondria narrower. (**D**). Average length of cristae measured on TEM sections from at least three independent stage 12–13 embryos (ventral epidermis). The average length of cristae is significantly increased in *PMI* mutant mitochondria ($n=66$ mitochondria) compared with those of wild-type ($n=91$), *drp1* ($n=20$) and *opa1* ($n=15$) genotypes. Consistently, restoring PMI expression rescues the crista phenotype of *PMI* mutant embryos (*PMI+*). Overexpressing PMI in a wild-type background by the mean of two *UAS-PMI* transgenes activated by a *da-GAL4* driver (*da-GAL4 UAS-PMI*; $n=75$) significantly reduced crista length compared to wild-type, *drp1* and *opa1* genotypes. Statistical significance was analysed by ANOVA ($P<0.0001$) followed by Tukey HSD *post hoc* test (***$P<0.001$). (**E**) For each *PMI* mutant mitochondrion analysed, the length of the longer cristae (µm) was plotted against the mitochondrial diameter (µm; $n=66$ mitochondria from four independent stage 12–13 *PMI* mutant embryos). (**F**) For each analysed mitochondrion the lengths of all the cristae were added together and multiplied by 2 to estimate the total length of the crista membrane per mitochondrion. We divide the total length of the membrane by the mitochondrion perimeter to obtain a crista membrane/outer membrane ratio (*c.m./o.m.*). The average *c.m./o.m.* ratio is higher in *PMI* mutant flies compared with wild-type, *drp1*, and *opa1* genotypes. Expression of a *PMI* rescue transgene in *PMI* mutant embryos (*PMI+*) restores a normal *c.m/o.m.* ratio. Overexpressing PMI in a wild-type background (*da-GAL4 UAS-PMI*) significantly reduced the *c.m./o.m.* ratio compared to the wild-type, *drp1* and *opa1* genotypes. Statistical significance was analysed by ANOVA ($P<0.0001$) followed by Tukey HSD *post hoc* test (***$P<0.001$). (**G**) The average crista sinuosity was determined for each crista by measuring the deviation between the actual crista length and the length of a straight line linking each extremity of the crista. No significant difference was observed between *PMI* and wild-type cristae (wild type $n=91$ mitochondria, *PMI* $n=66$ mitochondria, four independent stage 12–13 embryos analysed for each genotype). (**H**) The diameter of crista tubules (nm) was measured on electron microscopy sections of mitochondria. No significant difference was observed in *PMI* mutants. (**I**) High magnification electron microscopy image showing that *PMI* mutant mitochondria have well-formed crista junctions (cj). Cm, cristae membrane; om, outer membrane; imb, inner membrane boundary; ma, mitochondrial matrix.

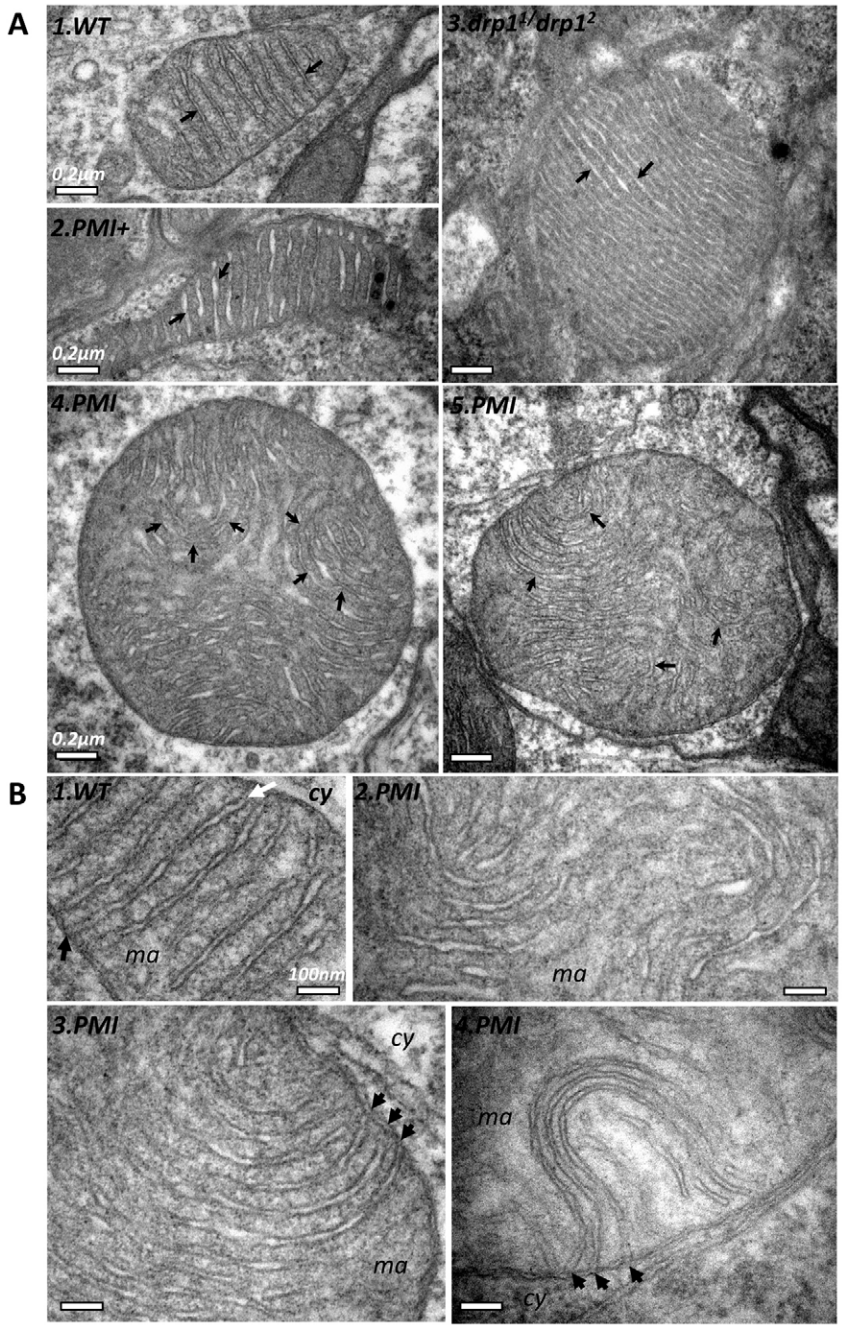

Fig. 2. Crista morphology is altered in *PMI* mutant flies. TEM images of adult fly brain sections showing mitochondria within neuron cell bodies. (**A**) *PMI* (4, 5) and *drp1*^{1}/*drp1*^{2} (3) mutant mitochondria are both enlarged and rounded compared with control mitochondria (1). In wild-type and *drp1*^{1}/*drp1*^{2} mitochondria, cristae are straight and parallel (1, 3, arrows) whereas the inner-membrane network in *PMI* mutant mitochondria is highly folded and disorganised and is often arranged into concentric stacks (4, 5, arrows). The *PMI* mitochondrial phenotype is rescued in the control *PMI*+ line (2) in which a genomic fragment containing the wild-type *PMI* sequence was inserted to restore PMI expression. (**B**) High magnification of mitochondria revealing crista morphology. In wild type, the electron dense inner-membrane invaginates to form cristae, the poorly electron-dense lumen of the cristae is connected to the inter-membrane space via crista junctions (B1, black arrow), crista tubules are closed by crista tips (1, white arrow). *PMI* mutant mitochondria have bent (2, 3) and even folded (4) crista membranes often arranged as concentric stack at the periphery (3). *PMI* mutant mitochondria still form crista junctions (3, 4, black arrows). Cy, cytoplasm; ma, mitochondrial matrix. Scale bars: 0.2 µm (A); 100 n, (B).

knockdown or overexpressing myocytes (Fig. 3). Altogether, these results suggest that, by controlling the biogenesis of crista membranes, the inner-membrane protein PMI can influence the diameter and in turn the tubular shape of mitochondria.

PMI mutant mitochondria have impaired respiratory chain function

As we showed that PMI is required for normal crista organisation, we investigated whether PMI inactivation would affect the oxidative metabolism that takes place in the mitochondrial cristae. As shown in Fig. 4, ATP levels were significantly lower in extracts from *PMI* mutant than from control flies, a phenotype that could be rescued by genetically restoring PMI expression (Fig. 4A). A similar reduction was observed after treatment of the flies with the respiratory chain blocker Paraquat. We then quantified mitochondrial membrane potential ($\Delta\Psi$m) using JC1 dye that accumulates in the mitochondrial matrix as green monomers and aggregates into red oligomers proportionally to $\Delta\Psi$m strength (Smiley et al., 1991; Reers et al., 1995). As expected, treatment with the proton ionophore DNP strongly inhibits the formation of JC1 aggregates in adult flight muscle mitochondria (Fig. 4C). Similarly, loss of PMI function was associated with a reduction of JC1 aggregates in muscle mitochondria, a phenotype that could be rescued by restoring PMI expression (Fig. 4B,C). Since the proton gradient is generated by the redox activity of the electron transport chain

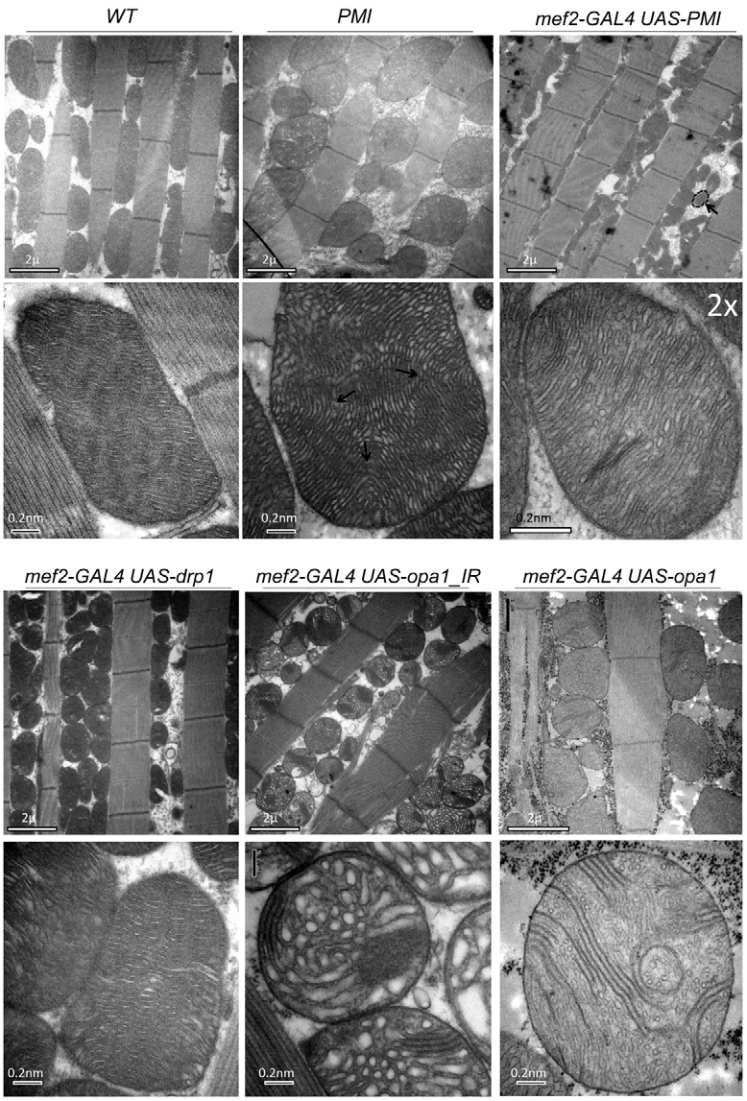

Fig. 3. PMI expression level influences mitochondrial diameter. Representative TEM images of adult flight muscles (DLM) showing mitochondrial morphology (top, low magnification images) and crista ultrastructure (bottom, high magnification images). In wild-type muscle mitochondria, cristae are evenly spaced and form a dense stack of wavy parallel membranes (bottom panel). In contrast, *PMI* mutant mitochondria, which are enlarged (top panels), have elongated crista membranes, which can bend and form concentric swirls (bottom panel, arrows). In contrast, overexpression of PMI by means of the *mef2-GAL4* muscle-specific driver (*mef2-GAL4 UAS-PMI*) dramatically reduces the overall size of the mitochondria (top panel, arrow), and alters cristae, which appear as short tubules scattered within the mitochondrion (*mef2-GAL4 UAS-PMI*, bottom panel; note that the size of the image was doubled). Those alterations in the cristae were not a consequence of reduced mitochondrial size as the overexpression of the fission effector *drp1* (*mef2-GAL4 UAS-drp1*), which induces mitochondria fragmentation (top panel), does not affect crista organisation and morphology (bottom panel). As previously reported (Frezza et al., 2006), downregulation of the inner-membrane fusion protein *opa1* (*mef2-GAL4 UAS-opa1_IR*) results in mitochondrial fragmentation and strongly increased crista width (bottom panel). Overexpression of *opa1* triggers complex mitochondrial abnormalities (*mef2-GAL4 UAS-opa1*). The mitochondria can be either enlarged or smaller, and the cristae display a variety of defects such as vacuolisation and membrane stacking or swirling. Those phenotypes were not observed in *PMI* mutant or overexpressing flies.

(ETC) complexes, we measured state III respiration in adult fly extracts, and found that the activity of mitochondrial complex I and II was significantly decreased in *PMI* mutants (Fig. 4D). This correlated with a decrease in the protein levels of ETC subunits from complex I and II in the absence of transcriptional repression, loss of mitochondrial DNA, or downregulation of the inner-membrane-associated protein ATP-synthase (supplementary material Fig. S4). Finally, as respiratory chain defects could result in the release of reactive oxygen species (ROS), we compared ROS production in wild-type and *PMI* mutants using the dihydroethidium (DHE) dye whose fluorescence is directly proportional to the level of superoxide free radicals. ROS levels measured in *PMI* mutant adult fly brains (Fig. 4E,F) were higher than in controls, consistent with results obtained with brains treated with Paraquat. It is noteworthy that in *drp1* mutants mitochondria, which are as large as *PMI* mitochondria but whose crista organisation is normal, ATP levels, $\Delta\Psi$m strength and ROS levels were not affected (Fig. 4A,C,F). This suggested that the alterations in ATP levels, ROS production and $\Delta\Psi$m detected in *PMI* mutant mitochondria are a consequence of altered crista shape and architecture rather than an effect of the overall mitochondrial size increase. Taken together, these results demonstrate that respiratory chain function relies on *PMI*-dependent crista morphogenesis.

PMI mutant flies have a reduced lifespan

Having characterised the consequences of the *PMI* mutation at the subcellular level and more specifically on mitochondrial shape and structure, we analysed the impact of inactivating PMI function at the organism level. The first noticeable phenotype was a reduction of the lifespan of *PMI* mutants. Whereas the median survival of wild-type animals reaches 50 days, it dropped to 13 days in *PMI* mutant flies, a phenotype greatly improved by restoring PMI expression (Fig. 5A). This premature death was not due to increased mitochondria size since *drp1* inactivation did not result in such premature adult lethality (Fig. 5A). In addition, the fact that brains and muscles from aged *PMI* flies did not show any sign of degeneration (vacuolization, apoptotic nuclei) or mitochondrial damages (supplementary material Fig. S1A–C), led us to suspect that adult lethality could be secondary to the increased ROS levels. This hypothesis was validated by

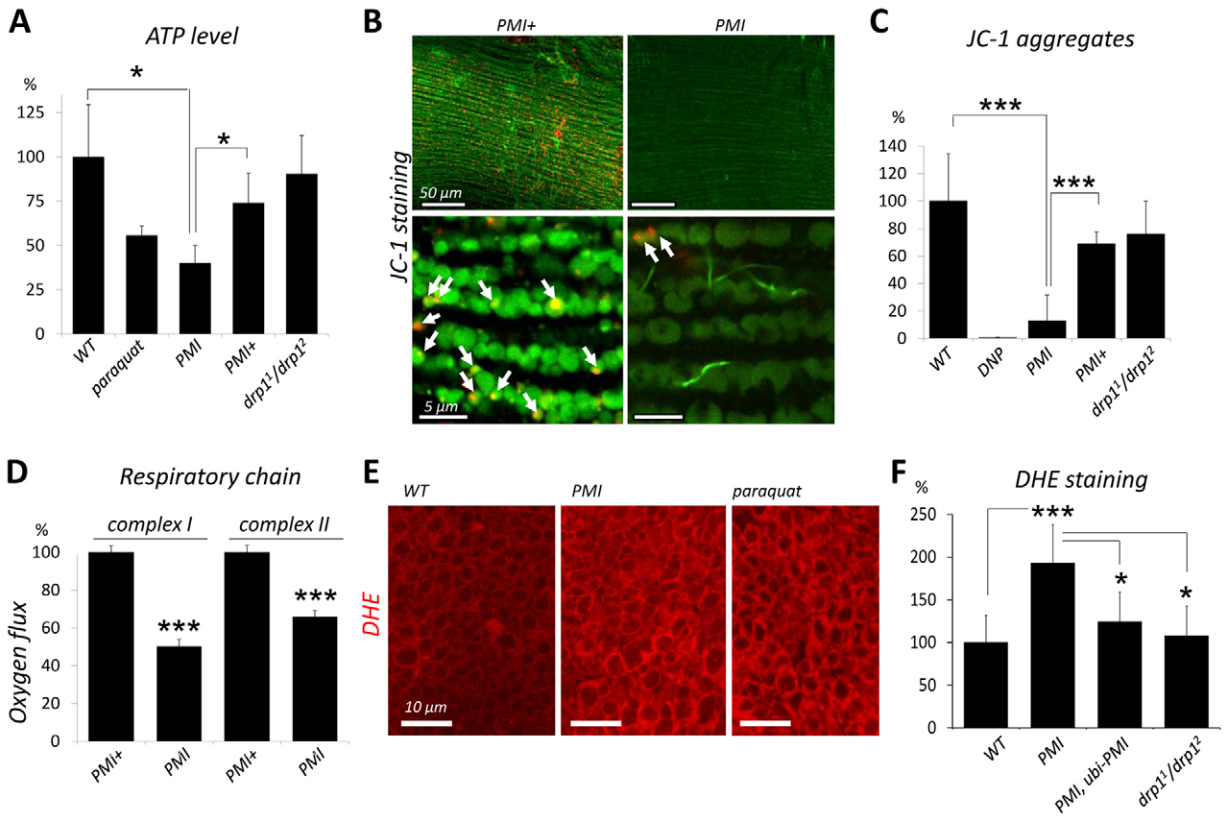

Fig. 4. Altered respiratory chain activity in *PMI* mutants. (**A**) Histogram showing the mean ATP concentration of adult fly extracts expressed as a percentage of controls. In wild-type flies poisoned with the respiratory chain blocker Paraquat the ATP level is reduced. *PMI* mutant flies have significantly less ATP than wild-type flies. This is rescued in the control *PMI+* line in which a genomic fragment containing the wild-type *PMI* sequence was inserted (see Materials and Methods for details). Inactivation of *drp1* does not affect the ATP level. Bars represent the standard error from six independent extracts of five flies. Statistical significance was analysed by ANOVA ($P=0.045$) followed by a Tukey HSD *post hoc* test (*$P<0.05$). (**B**) Confocal images of adult flight muscles stained with the JC-1 probe. JC-1 monomers (green channel) accumulate into the mitochondria proportionally to the strength of the mitochondrial membrane potential. The accumulation of JC-1 ultimately results in the formation of JC-1 aggregates (red channel, arrows). Bottom panels show higher magnification views. *PMI* loss-of-function results in decreased JC-1 accumulation in mitochondria (green) and decreased formation of JC-1 aggregates (red, arrows) compared with control *PMI+* rescue flies. (**C**) Histogram showing the average number of JC-1 aggregates per mm^2 of whole-mount adult flight muscles (percentage of control). Treatment, with DNP, which dissipates the mitochondrial proton gradient, inhibits the formation of JC-1 aggregates, as does the inactivation *PMI*. Restoring the expression of *PMI* significantly increases the formation of JC-1 aggregates (*PMI+*). Inactivation of *drp1* has no significant effect ($drp1^1/drp1^2$). Bars represent the standard error of three independent experiments involving a minimum of 10 independent muscles. Statistical significance was analysed by ANOVA ($P=0.00{,}025$) followed by a Tukey HSD *post hoc* test (***$P<0.001$). (**D**) Activity of the respiratory chain complex I and complex II measured on adult fly extracts by high-resolution respirometry (pmol/s/ml). Values are the mean oxygen flux as a percentage of the control ($n=17$ independent extracts for each genotype for complex I and $n=10$ independent extracts for each genotype for complex II). *PMI* mutant flies show significant decreased respiratory activity for both CI and CII compared with control *PMI+* rescued flies. Statistically significant values are indicated by asterisks (unpaired Student's *t*-test, ***$P<0.0001$). (**E**) Adult fly brains stained with DHE. Increased DHE staining is detected in *PMI* mutant flies or in flies fed with the respiratory chain toxin Paraquat. (**F**) Histogram showing to the mean DHE staining intensity expressed as percentage of controls. Increased DHE staining is detected in *PMI* but *drp1* mutant brains. Restoring *PMI* expression significantly decreases superoxide release in *PMI* mutant flies (*PMI, ubi-PMI*). Bars represent the standard error of a minimum of four independent experiments involving, in total, a minimum of 10 brains. Statistical significance was analysed by ANOVA ($P<0.0001$) followed by a Tukey HSD *post hoc* test (*$P<0.05$, ***$P<0.001$).

experiments showing that overexpression of the mitochondrial specific anti-oxidant protein Mn-superoxide dismutase (SOD2) significantly increased median survival of *PMI* mutant (Fig. 5B). These results demonstrate that *PMI* mutant premature lethality is partly the consequence of excessive ROS production by *PMI* mutant mitochondria. It should be noted that SOD2 overexpression did not rescue mitochondrial defects, indicating that abnormal mitochondrial morphology is not caused by an excess of ROS (supplementary material Fig. S5). These results demonstrate that *PMI*-dependent alterations at the mitochondrial level dramatically impair survival at the organism level.

Impaired neuronal activity in *PMI* mutant flies

We then tested whether *PMI* loss-of-function mutation could impair neuronal activity, which strongly relies on mitochondria for energy supply and calcium buffering. Behavioural and locomotion tests were applied to both wild-type and *PMI* mutant flies. When performing these tests, we observed that *PMI* mutants were paralyzed when submitted to a stressful mechanical shock. This phenotype, known as bang sensitive, has been described for *Drosophila* mutants affecting certain aspect of mitochondria function (Fig. 6A; supplementary material Movie S1). We therefore measured the synaptic activity at the neuromuscular junction of *PMI* mutant flies using a well-established protocol

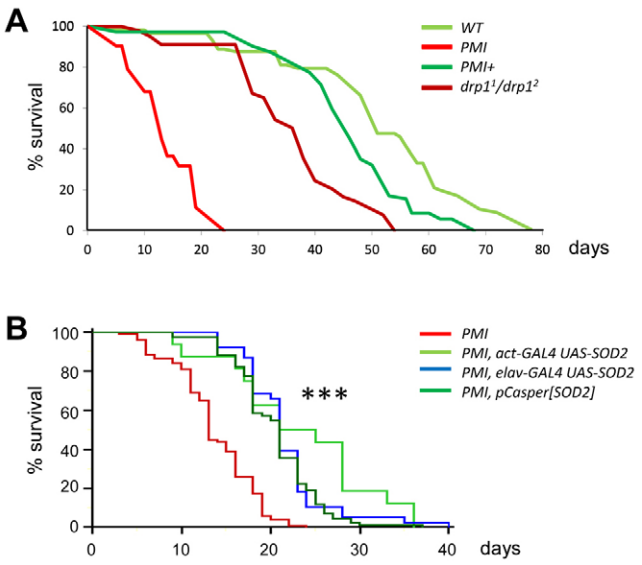

Fig. 5. Decreased lifespan in *PMI* mutant flies. (**A**) Lifespan recording of adult flies. The median survival of *PMI* mutants drops to 13 days versus 50 days in controls. Insertion of a wild-type *PMI* genomic construct restores survival rate (*PMI+*). In contrast to the *PMI* mutation, the impact of *drp1* inactivation on lifespan is moderate ($drp1^1/drp1^2$). (**B**) Expression of the mitochondrial superoxide dismutase (SOD2) ubiquitously (by the mean of the *actin-GAL4* driver: *PMI, act-GAL4 UAS-SOD2* or of a genomic transgene: *PMI, pCasper[SOD2]*), or only in neurons (*PMI, elav-GAL4 UAS-SOD2*) extends the lifespan of *PMI* mutant flies. Statistical significance was analysed by a Log rank test (***$P<0.001$).

(Tanouye and Wyman, 1980; Elkins and Ganetzky, 1990; Dupont et al., 2012). Although *PMI* mutants were able to generate excitatory post-synaptic potential (EPSP), a higher rate of EPSP failure was detected in these flies (Fig. 6B,C). Both bang sensitivity and impaired neuronal activity were rescued by specifically targeting PMI expression into neurons (Fig. 6A,C), consistent with the tissue-specific restoration of mitochondrial morphology (supplementary material Fig. S2). Although reduced ATP production by *PMI* mutant mitochondria probably contributes to the synaptic defects observed, we asked whether PMI inactivation could also affect the transport of mitochondria to synapses. Indeed, although *drp1* mutant flies have normal ATP levels, their mitochondria are too massive to be transported to synapses, resulting in bang sensitivity and impaired neuronal activity (Fig. 6A) (Verstreken et al., 2005). We therefore imaged optic lobes that contain a regular succession of cortical and neuropil layers made up of cell bodies and synapses. Whereas mitochondria were highly enriched in the neuropil layers of controls, their density was reduced in neuropils and increased in cell bodies of PMI mutants (Fig. 6D; supplementary material Fig. S6). These phenotypes were restored by targeting PMI expression in neurons (supplementary material Fig. S6B,D). In conclusion, PMI-dependent mitochondrial morphogenesis is required for neuronal activity, efficient transport of mitochondria to synapses, and in consequence, for normal behaviour.

Discussion

PMI controls cristae length and organisation

Our results show that the mitochondria inner-membrane protein *PMI* plays a central role in regulating crista morphology. Could this function be related to mechanisms previously described for other inner-membrane proteins? It was recently reported that loss-of-function mutants for Mitofilin or proteins of the MitOS/MICOS/MINOS complex are devoid of crista junctions and have closed cristae (Rabl et al., 2009; Harner et al., 2011; Hoppins et al., 2011; von der Malsburg et al., 2011). In contrast, Mitofilin overexpression causes crista branching, supporting the idea that Mitofilin might negatively bend membranes to maintain crista junction integrity (Rabl et al., 2009). None of these phenotypes were observed in *PMI* mutant mitochondria. Consistently, our previous data have shown that PMI associated with crista tubules and not to crista junctions (Rival et al., 2011). These data suggest that PMI is probably not a protein involved in the maintenance of crista junctions. The e and g non-catalytic subunits of F0F1 ATP synthase are two other well-characterised determinants of crista morphology. Yeast mutants for these proteins exhibit branched and even concentric (or 'onion-like') crista tubules, which probably result from fusion of cristae (Paumard et al., 2002; Rabl et al., 2009; Velours et al., 2009). It has been proposed that by creating membrane constraints, F0F1 e/g su shape crista tips and prevent inter-crista fusion (Rabl et al., 2009; Velours et al., 2009). As for F0F1 e/g su mutants, *PMI* mutant mitochondria contain highly bent cristae in adult neurons. However, although *PMI* mutant cristae can form hemi-concentric stacks of membrane that partly evoke the onion-like structure, they appear as a disorganised tangle of membranes that are never branched or interconnected. This suggests that PMI is regulating crista shape by a mechanism independent of F0F1 e/g su. How are the cristae maintained as straight and not bent entities? It was recently proposed that the negative and positive bending activities of Mitofilin and F0F1 e/g su, respectively, could antagonize each other to perform this function (Rabl et al., 2009). This model does not exclude the possibility that proteins whose function is to straighten the crista membranes exist. Given that loss of the PMI in adult neurons results in crista bending, it is tempting to propose that PMI could be one of these putative straightening factors. However, the analysis of cristae in *PMI* mutant embryo does not support this hypothesis. Although mitochondria cristae in embryos are highly elongated, they are still able to form straight and evenly spaced parallel tubules. Moreover, PMI overexpression in embryonic and in adult tissues provokes a reduction of the cristae length. These results suggest that the *PMI* mutant phenotype results from the over-growth of crista membranes that create hyper-elongated tubules. In this case, the phenotype observed in adult neurons would be the result of the cumulative effects of the uncontrolled crista growth during the course of development. We therefore propose that *PMI* controls the elongation of crista tubules by negatively regulating membrane biogenesis.

Respiratory chain function requires PMI

PMI mutant flies exhibit striking signs of altered oxidative metabolism including decreased respiratory activity, weaker $\Delta\Psi m$, decreased ATP production and increased production of ROS. What could be the link(s) between PMI inactivation and respiratory chain dysfunction? The overall size increase and the abnormal cytoplasmic distribution of *PMI* mutant mitochondria are not likely to be involved since *drp1* mutant mitochondria, which share similar defects, do not have altered oxidative metabolism (our data Fig. 4, and Ishihara et al., 2009; Wakabayashi et al., 2009). Since cristae concentrate respiratory

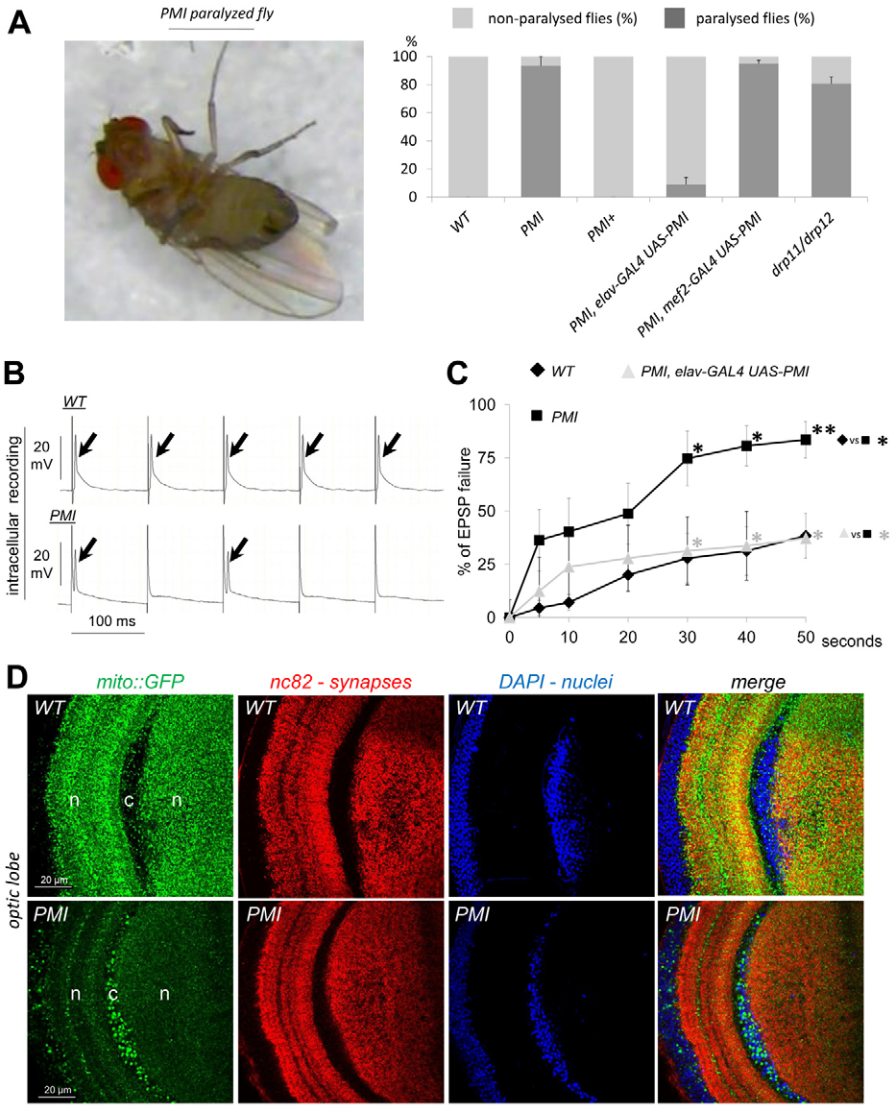

Fig. 6. Synaptic defects and impaired mitochondrial transport in *PMI* mutant flies. (**A**) Homozygous *PMI* mutants develop normally until adulthood but are bang sensitive (right panel), meaning that they are paralysed by a mechanical shock and lie on their back for a couple of minutes before recovering. Histograms show quantitative analysis of the bang sensitive phenotype (light and dark grey bars correspond, respectively, to the percentage of moving and paralysed flies). When submitted to a 20-second vortex, 90% of the *PMI* mutant flies are left paralyzed ($n=58$) versus none in controls ($n=61$ flies). This is efficiently rescued by restoring *PMI* expression (*PMI+*). Bang sensitivity could also be abolished by providing *PMI* specifically to neurons (*PMI, elav-GAL4 UAS-PMI*, $n=57$). In controls, expression of a *UAS-PMI* transgene in muscles has no effect (*PMI, mef2-GAL4 UAS-PMI*, $n=41$). $drp1^{1}/drp1^{2}$ mutants also display a similar bang sensitivity ($n=21$). (**B**) Electrophysiological recording of flight muscle potentials (EPSP) following stimulations of the giant fibre pathway. 10 V stimulations were applied at 10 Hz frequency, and the evoked EPSPs were recorded. The two recordings show representative intracellular responses of wild-type and *PMI* mutant muscles during 5 seconds of stimulation. On each trace, the first short spike corresponds to the stimulation artefact, and the second to the EPSP (arrow). (**C**) Graph showing the rate of EPSP failure during 50 seconds of constant 10 Hz stimulation. From the first 5 seconds of stimulation, the rate of EPSP failure increases more rapidly in *PMI* mutant flies than in controls. After 30 seconds, 75% of the stimulations failed to induce an EPSP in mutants compared to 25% in control animals. Expression of PMI specifically in neurons can restore a normal rate of EPSP response (*PMI, elav-GAL4 UAS-PMI*). The number of independent flies recorded was: wt, $n=8$; *PMI*, $n=8$; *PMI, elav-GAL4 UAS-PMI*, $n=6$). For each time point, statistical significance was analysed by ANOVA followed by a Tukey HSD *post hoc* test (*$P<0.05$, **$P<0.01$). (D) *elav-GAL4 UAS-mito::GFP* optic lobes stained with a synapse-specific antibody (anti-nc82) and DAPI. Whereas mitochondria are located at the synapses in control neuropils (n), they concentrate into neuronal cell bodies (c) and are hardly detected in synaptic area (n) in *PMI* mutants.

chain complexes (Gilkerson et al., 2003; Vogel et al., 2006; Wurm and Jakobs, 2006), it is possible that abnormal crista morphogenesis alters the crista membrane micro-environment and in turns impairs oxidative metabolism. Consistently, in Mitofilin mutants, loss of crista junctions results in defective oxidative metabolism (John et al., 2005; Rabl et al., 2009). Similar observations were made in cells mutant for the cristae-associated proteins OPA1 and Prohibitin (Schleicher et al., 2008; Zanna et al., 2008; Osman et al., 2009a). Our finding that protein but not mRNA level of ETC subunits is decreased in *PMI* mutant flies supports this hypothesis. Indeed, the aberrant crista membrane organisation triggered by loss of PMI might affect

membrane insertion of the respiratory chain complexes, resulting in their degradation. This, however, does not reflect a general destabilisation of the inner membrane protein pool since ATP synthase is not affected. Finally, in contrast to F0F1 e/g su mutants in which loss of mtDNA affect oxidative metabolism (Paumard et al., 2002), mtDNA content was not significantly altered in *PMI* mutants. These data support the idea that different defects in crista membrane organization can have specific impacts on mitochondrial function.

PMI-dependent inner-membrane organisation supports the tubular shape of mitochondria

Loss of PMI has not only consequences on inner-membrane organisation but also on the overall shape of the mitochondrion. *PMI* mutant mitochondria lose their tubular shape and become spherical, a phenotype that does not result from defective fission or unbalanced fusion (Rival et al., 2011). This is consistent with the fact that although *drp1* and *PMI* mutant mitochondria look much alike in adult neurons, with a similar global shape and size, their crista morphology is very different. This difference is even more obvious at the onset of embryogenesis. Whereas in early embryos *PMI* mutant mitochondria form large spheres, *drp1* mutant mitochondria, although highly interconnected, remain tubular. In contrast, inhibition of *opa1* induces fragmentation of mitochondrial tubules into spherical entities whose diameter remains comparable to that of wild-type mitochondria. These experiments suggest that whereas fission and fusion control the length of the mitochondrial tubules, *PMI* controls the diameter. We therefore propose that the excessive crista elongation observed in *PMI* mutant mitochondria probably triggers the increased width and therefore the spherical shape of the overall organelle. This suggests that crista length determines mitochondrial diameter, and therefore that the usual tubular shape of mitochondria can be intrinsically determined by inner-membrane morphogenesis.

Materials and Methods

Drosophila stocks and culture

Generation of *PMI* mutant flies and control *PMI+* line is described in detailed in Rival et al. (Rival et al., 2011). Briefly, because *PMI* is encoded by a bicistronic locus together with the putative immune gene *PGRP-LD*, the genomic transgene *Pac[PMI*_PGRP-LD]*, in which only the *PMI* coding sequence is mutated, was inserted into *PMI* knock out flies at the *attp2* third chromosome landing site to generate a specific *PMI* mutant (*w; Df(PMI_PGRP-LD $^{p[w+]}$), Pac[PMI*_PGRP-LD]attp2*). In the *PMI+* line, a wild-type *Pac[PMI_PGRP-LD]* genomic transgene was inserted at the same chromosomal location to create a control rescue line (*w;; Df(PMI_PGRP-LD $^{p[w+]}$), Pac[PMI_PGRP-LD]attp2*). To overexpress PMI we generated flies stably carrying both *UAS-PMI attp40* (second chromosome) and *UAS-PMI attp2* (third chromosome) transgenes that were then crossed to GAL4 flies (Rival et al., 2011). Fly stocks carrying *drp1^{1}* and *drp1^{2}* alleles were from Dr P. Verstreken, *UAS-mnSOD2* from Prof. J. Phillips, *Pcasper[SOD2]* from Dr R. J. Mockett, *UAS-opa1_IR* from Dr M. Guo, and *UAS-opa1* from Prof. J. Chung. *UAS-mito::GFP* line, *sqh-mito::YFP*, *elav-GAL4*, *act5c-GAL4*, *hsp-FLP*, *FRT40A ovoD*, *opa1*, *da-GAL4* and *mef2-GAL4* lines were from the Bloomington Stock Center. *PMI* mutant embryos were obtained from homozygous *PMI* mutant females being therefore devoid of both maternal and zygotic PMI expression. We generated embryos devoid of *drp1* maternal contribution by crossing heat-shocked *w, hsp70-FLP; FRT40A, Ovo^{D}/FRT40A, drp1^{1}; sqh-mit::YFP* females to *w; FRT40A, drp1^{1}; sqh-mit::YFP* males. *Drosophila* stocks were maintained at 25℃ on a standard cornmeal agar diet.

Assay for bang sensitivity

A dozen age-matched flies (2- to 3-days old) were anesthetized and placed in a culture vial. After 30 minutes recovery from CO_2 exposure, the vial was vortexed for 10 seconds and the number of paralysed flies was immediately determined.

Longevity assays

Assays for longevity were performed on about 80 flies in groups of 10 in separate vials. Flies were kept at 25℃ on a standard cornmeal agar diet. All tubes were kept horizontally because *PMI* mutant flies have the tendency to stick in the medium when experiencing seizures. Viable flies were counted and their food changed on days 1, 3 and 5 of a 7-day cycle. Log rank statistical test were performed using the MedCalc software package.

Electrophysiology

Electrophysiological recordings from flight muscles were performed with intracellular electrodes essentially as described previously (Rival et al., 2006; Dupont et al., 2012). Age-matched adult female flies were fixed with cyanoacrylate adhesive at the extremity of a needle and the dorsal thoracic cuticle was removed to expose the dorso-longitudinal flight muscle (DLM). A 10 V electrical stimulation was applied to the brain with a pair of tungsten microelectrodes isolated from the ground. This stimulated the giant fibre pathway that includes the DLM motor neurons (Tanouye and Wyman, 1980; Elkins and Ganetzky, 1990).

In situ labelling

Primary antibodies used were: mouse anti-ATP synthase monoclonal antibody MS507 (MitoSciences; 1:300) for mitochondria; mouse anti-Bruchpilot nc82 monoclonal antibody (Hybridoma bank; 1:100) for synapses. Secondary antibodies: Alexa Fluor 488 goat anti-mouse IgG, Alexa Fluor 546 goat anti-mouse IgG.

For *in situ* detection of *mit::YFP*, embryos were dechorionized with bleach, glued onto a glass coverslip, and covered with oil to prevent desiccation. For *in situ* detection of mito::GFP, tissues were dissected in PBS, fixed for 15 minutes in 4% formaldehyde, and washed for 5 minutes. For immunolabelling, tissues were dissected in PBS, fixed for 30 minutes in 4% formaldehyde, washed for 5 minutes, permeabilised for 2 hours in 0.5% Triton X-100 in PBS, and saturated for 1 hour in 0.5% BSA, 0.1% Tween 20 in PBS (PBTB). Primary antibody diluted in PBTB was incubated overnight at 4℃, and later washed for 1 hour in 0.1% Tween 20 in PBS (PBTw). Secondary antibody was incubated for 2 hours and washed for 1 hour in PBTw. Preparations were mounted in Vectashield/DAPI (Vector). An LSM780 Zeiss confocal microscope was used for imaging.

Electron microscopy

Adult fly heads, thoraxes and embryos were fixed in 2% paraformaldehyde, 2.5% glutaraldehyde, 5 mM $CaCl_2$, 0.1 mM sodium cacodylate for 24 hours at 4℃. This was followed by 2-hour post-fixation in 2.5% glutaraldehyde, 0.8% osmium tetroxide, 0.1 mM sodium cacodylate at 4℃. Ultrathin Epon plastic sections were examined with a Leo 912 Zeiss microscope at 100 kV.

Superoxide staining with DHE

DHE staining was essentially performed as described previously (Owusu-Ansah et al., 2008). Tissues were dissected in PBS and incubated for 5 minutes in 30 µM DHE (in Schneider's medium) at room temperature, then washed and fixed for 8 minutes in 4% formaldehyde. DHE (excitation 350 nm, emission 430 nm) is oxidized by superoxide free radicals into ethidium (excitation 530 nm, emission 620 nm). The ethidium signal was detected with a LSM510 Meta confocal microscope (Zeiss) using a HeNe 543 nm laser, and a 560–660 nm window of detection. Pixel density was determined using ImageJ software.

JC-1 *in situ* labelling

Adult flight muscles (DLM) were rapidly dissected in Schneider's medium and incubated for 45 minutes, at room temperature, in 2 µM JC-1 solution (in 1% cyclodextrine Schneider's medium). Muscles mounted in Schneider's medium were immediately imaged with a LSM780 confocal microscope (Zeiss). For detection of green fluorescent monomers, and red fluorescent aggregate, excitation wavelengths were, respectively, 488 nm and 561 nm. A confocal image was taken of each prepared flight muscle, and the number of JC-1 red fluorescent aggregates automatically counted using ImageJ software.

Measurement of ATP concentration

Extracts from five adult flies were immediately deproteinised by perchloric acid precipitation (deproteinisation kit, Abcam) to eliminate ATP-consuming enzymes. ATP quantification was performed according to manufacturer's instruction (ATP fluorometric kit, Abcam). Fluorescence was measured with a Hitashi FL4500 fluorospectrophotometer (excitation/emission wavelengths: 535 nm/587 nm). Glycerol phosphate background was subtracted.

TUNEL staining

The Apoptag Red *In Situ* Detection Kit (Chemicon) was used to detect apoptotic nuclei in adult fly brains and flight muscles. Tissues were dissected and fixed in 4% formaldehyde in PBS. Fixed tissue were washed in PBS and apoptosis detected according to the manufacturer's instructions.

Respirometry analysis

Mitochondrial respiration was assayed at 37℃ by high-resolution respirometry using an OROBOROS Oxygraph. The DatLab software package (OROBOROS,

Innsbruck, Austria) was used for data acquisition (2-second time intervals) and analysis, including calculation of the time derivative of the oxygen concentration, signal deconvolution dependent on the response time of the oxygen sensor and correction for instrumental background oxygen flux. State III respiration was assayed by homogenising two flies using a pestle in MiR05 respiration buffer (20 mM HEPES, 10 mM KH_2PO_4, 110 mM sucrose, 20 mM taurine, 60 mM potassium lactobionate, 0.5 mM EGTA, 3 mM $MgCl_2$, 1 g/l fatty-acid-free BSA) in the presence of 5–10 mM ADP. In particular, respiration buffer was supplemented with 2 mM malate plus 10 mM glutamate for complex I activity measurements and 1 mM rotenone plus 10 mM succinate for complex II activity measurements.

Protein extraction and western blotting

Protein extracts from adult flies were prepared by grinding flies in lysis buffer [25 mM Tris-HCl pH 7.4, 300 mM NaCl, 5 mM EDTA, 10% (w/v) SDS, 1 mM PMSF, 0.5% (w/v) Nonidet-40] containing the protease inhibitors leupeptin, antipain, chymostatin, pepstatin (Sigma) at the manufacturer's recommended dilution. The suspensions were cleared by centrifugation at 15,700 ***g*** for 10 minutes at 4℃ and supernatants were mixed with 2× SDS loading buffer. For SDS-PAGE equivalent volumes of protein lysates were resolved on 10% Precast Gels (Invitrogen) and transferred onto nitrocellulose membranes. The membranes were blocked in TBS [0.15 M NaCl, 10 mM Tris-HCl (pH 7.5)] containing 5% (w/v) dried nonfat milk (blocking solution) for 1 hour at room temperature, and probed with the indicated primary antibody before being incubated with the appropriate HRP-conjugated secondary antibody. Antibody complexes were visualized by Pierce enhanced chemiluminescence (ECL). Primary antibodies employed in this study were OXPHOS rodent cocktail 1:1000 (Mitosciences), ATP synthase subunit alpha 1:1000 (Mitosciences) and α-tubulin 1:5000 (Sigma).

mtDNA quantification

Analysis of mitochondrial DNA content was performed by quantitative real-time PCR on an Mx4000 real-time cycler (Stratagene) using the QuantiTect SYBR Green PCR system (Qiagen). Specific primers for mitochondrial DNA (Fw primer: 5′-CAACCATTCATTCCAGCCTT-3′ and Rev primer: 5′-GAAAATTTTA-AATGGCCGCA-3′) were designed using the primer-BLAST tool (NCBI). The relative levels of mitochondrial DNA were normalised to nuclear DNA using primers to *dmActin* (Dm_Act79B, QuantiTect Primer Assay, Cat. No. QT00967393). Quantification was performed using the comparative Ct method.

Quantitative real-time PCR

qRT-PCRs were performed on adult fly mRNA extracts. The following primers were used: 5′-CCAGGAAGCAGGCAAAGTAG-3′ and 5′-ATGGTCTGGGCTA-CGGAGAT-3′ for *NDUFb8/CG3192*, and 5′-CTACGAGCAGTACCGCAACA-3′ 5′-AGTCGATGATCCAGCGGTAG-3′ for *SDHb/CG3283*. The amount of mRNA detected was normalized to control *rp49* mRNA values (5′-GACGCTTCAAGGGACAGTATCTG-3′ and 5′-AAACGCGGTTCTGCATGA-3′). Normalized data were used to quantify the relative levels of a given mRNA according to cycling threshold analysis (ΔCt).

Acknowledgements

We thank J. P. Chauvin, A. Aouane, and F. Richard (IBDML) for electron microscopy, Dr J. Devaux (CRN2M) for analysis of electrophysiological recordings, Prof. P. Belenguer and Dr L. Arnauné for helpful discussion and comments on the manuscript, and C. Nguyen for measurement and quantification on EM images.

Funding

This work was supported by the Centre National de la Recherche Scientifique; the Agence Nationale de la Recherche (ANR-blanc); and the Association Française contre les Myopathies.

Supplementary material available online at
http://jcs.biologists.org/lookup/suppl/doi:10.1242/jcs.115675/-/DC1

References

Acehan, D., Xu, Y., Stokes, D. L. and Schlame, M. (2007). Comparison of lymphoblast mitochondria from normal subjects and patients with Barth syndrome using electron microscopic tomography. *Lab. Invest.* **87**, 40-48.

Baloyannis, S. J. (2006). Mitochondrial alterations in Alzheimer's disease. *J. Alzheimers Dis.* **9**, 119-126.

Celotto, A. M., Frank, A. C., McGrath, S. W., Fergestad, T., Van Voorhies, W. A., Buttle, K. F., Mannella, C. A. and Palladino, M. J. (2006). Mitochondrial encephalomyopathy in Drosophila. *J. Neurosci.* **26**, 810-820.

Chung, M. J. and Suh, Y. L. (2002). Ultrastructural changes of mitochondria in the skeletal muscle of patients with amyotrophic lateral sclerosis. *Ultrastruct. Pathol.* **26**, 3-7.

Cipolat, S., Rudka, T., Hartmann, D., Costa, V., Serneels, L., Craessaerts, K., Metzger, K., Frezza, C., Annaert, W., D'Adamio, L. et al. (2006). Mitochondrial rhomboid PARL regulates cytochrome c release during apoptosis via OPA1-dependent cristae remodeling. *Cell* **126**, 163-175.

Detmer, S. A. and Chan, D. C. (2007). Functions and dysfunctions of mitochondrial dynamics. *Nat. Rev. Mol. Cell Biol.* **8**, 870-879.

Dimmer, K. S., Jakobs, S., Vogel, F., Altmann, K. and Westermann, B. (2005). Mdm31 and Mdm32 are inner membrane proteins required for maintenance of mitochondrial shape and stability of mitochondrial DNA nucleoids in yeast. *J. Cell Biol.* **168**, 103-115.

Dimmer, K. S., Navoni, F., Casarin, A., Trevisson, E., Endele, S., Winterpacht, A., Salviati, L. and Scorrano, L. (2008). LETM1, deleted in Wolf-Hirschhorn syndrome is required for normal mitochondrial morphology and cellular viability. *Hum. Mol. Genet.* **17**, 201-214.

Dupont, P., Besson, M. T., Devaux, J. and Liévens, J. C. (2012). Reducing canonical Wingless/Wnt signaling pathway confers protection against mutant Huntingtin toxicity in Drosophila. *Neurobiol. Dis.* **47**, 237-247.

Dürr, M., Escobar-Henriques, M., Merz, S., Geimer, S., Langer, T. and Westermann, B. (2006). Nonredundant roles of mitochondria-associated F-box proteins Mfb1 and Mdm30 in maintenance of mitochondrial morphology in yeast. *Mol. Biol. Cell* **17**, 3745-3755.

Elkins, T. and Ganetzky, B. (1990). Conduction in the giant nerve fiber pathway in temperature-sensitive paralytic mutants of Drosophila. *J. Neurogenet.* **6**, 207-219.

Frey, T. G. and Mannella, C. A. (2000). The internal structure of mitochondria. *Trends Biochem. Sci.* **25**, 319-324.

Frezza, C., Cipolat, S., Martins de Brito, O., Micaroni, M., Beznoussenko, G. V., Rudka, T., Bartoli, D., Polishuck, R. S., Danial, N. N., De Strooper, B. et al. (2006). OPA1 controls apoptotic cristae remodeling independently from mitochondrial fusion. *Cell* **126**, 177-189.

Gilkerson, R. W., Selker, J. M. and Capaldi, R. A. (2003). The cristal membrane of mitochondria is the principal site of oxidative phosphorylation. *FEBS Lett.* **546**, 355-358.

Harner, M., Körner, C., Walther, D., Mokranjac, D., Kaesmacher, J., Welsch, U., Griffith, J., Mann, M., Reggiori, F. and Neupert, W. (2011). The mitochondrial contact site complex, a determinant of mitochondrial architecture. *EMBO J.* **30**, 4356-4370.

Hasegawa, A. and van der Bliek, A. M. (2007). Inverse correlation between expression of the Wolfs Hirschhorn candidate gene Letm1 and mitochondrial volume in C. elegans and in mammalian cells. *Hum. Mol. Genet.* **16**, 2061-2071.

Head, B. P., Zulaika, M., Ryazantsev, S. and van der Bliek, A. M. (2011). A novel mitochondrial outer membrane protein, MOMA-1, that affects cristae morphology in Caenorhabditis elegans. *Mol. Biol. Cell* **22**, 831-841.

Hoppins, S., Collins, S. R., Cassidy-Stone, A., Hummel, E., Devay, R. M., Lackner, L. L., Westermann, B., Schuldiner, M., Weissman, J. S. and Nunnari, J. (2011). A mitochondrial-focused genetic interaction map reveals a scaffold-like complex required for inner membrane organization in mitochondria. *J. Cell Biol.* **195**, 323-340.

Ishihara, N., Nomura, M., Jofuku, A., Kato, H., Suzuki, S. O., Masuda, K., Otera, H., Nakanishi, Y., Nonaka, I., Goto, Y. et al. (2009). Mitochondrial fission factor Drp1 is essential for embryonic development and synapse formation in mice. *Nat. Cell Biol.* **11**, 958-966.

John, G. B., Shang, Y., Li, L., Renken, C., Mannella, C. A., Selker, J. M., Rangell, L., Bennett, M. J. and Zha, J. (2005). The mitochondrial inner membrane protein mitofilin controls cristae morphology. *Mol. Biol. Cell* **16**, 1543-1554.

Mannella, C. A. (2006a). The relevance of mitochondrial membrane topology to mitochondrial function. *Biochim. Biophys. Acta* **1762**, 140-147.

Mannella, C. A. (2006b). Structure and dynamics of the mitochondrial inner membrane cristae. *Biochim. Biophys. Acta* **1763**, 542-548.

Meeusen, S., DeVay, R., Block, J., Cassidy-Stone, A., Wayson, S., McCaffery, J. M. and Nunnari, J. (2006). Mitochondrial inner-membrane fusion and crista maintenance requires the dynamin-related GTPase Mgm1. *Cell* **127**, 383-395.

Mitra, K., Wunder, C., Roysam, B., Lin, G. and Lippincott-Schwartz, J. (2009). A hyperfused mitochondrial state achieved at G1-S regulates cyclin E buildup and entry into S phase. *Proc. Natl. Acad. Sci. USA* **106**, 11960-11965.

Mitra, K., Rikhy, R., Lilly, M. and Lippincott-Schwartz, J. (2012). DRP1-dependent mitochondrial fission initiates follicle cell differentiation during Drosophila oogenesis. *J. Cell Biol.* **197**, 487-497.

Mun, J. Y., Lee, T. H., Kim, J. H., Yoo, B. H., Bahk, Y. Y., Koo, H. S. and Han, S. S. (2010). Caenorhabditis elegans mitofilin homologs control the morphology of mitochondrial cristae and influence reproduction and physiology. *J. Cell. Physiol.* **224**, 748-756.

Nunnari, J. and Suomalainen, A. (2012). Mitochondria: in sickness and in health. *Cell* **148**, 1145-1159.

Okamoto, K. and Shaw, J. M. (2005). Mitochondrial morphology and dynamics in yeast and multicellular eukaryotes. *Annu. Rev. Genet.* **39**, 503-536.

Olichon, A., Baricault, L., Gas, N., Guillou, E., Valette, A., Belenguer, P. and Lenaers, G. (2003). Loss of OPA1 perturbates the mitochondrial inner membrane structure and integrity, leading to cytochrome c release and apoptosis. *J. Biol. Chem.* **278**, 7743-7746.

Osman, C., Merkwirth, C. and Langer, T. (2009a). Prohibitins and the functional compartmentalization of mitochondrial membranes. *J. Cell Sci.* **122**, 3823-3830.

Osman, C., Haag, M., Potting, C., Rodenfels, J., Dip, P. V., Wieland, F. T., Brügger, B., Westermann, B. and Langer, T. (2009b). The genetic interactome of prohibitins: coordinated control of cardiolipin and phosphatidylethanolamine by conserved regulators in mitochondria. *J. Cell Biol.* **184**, 583-596.

Owusu-Ansah, E., Yavari, A., Mandal, S. and Banerjee, U. (2008). Distinct mitochondrial retrograde signals control the G1-S cell cycle checkpoint. *Nat. Genet.* **40**, 356-361.

Paumard, P., Vaillier, J., Coulary, B., Schaeffer, J., Soubannier, V., Mueller, D. M., Brèthes, D., di Rago, J. P. and Velours, J. (2002). The ATP synthase is involved in generating mitochondrial cristae morphology. *EMBO J.* **21**, 221-230.

Rabl, R., Soubannier, V., Scholz, R., Vogel, F., Mendl, N., Vasiljev-Neumeyer, A., Körner, C., Jagasia, R., Keil, T., Baumeister, W. et al. (2009). Formation of cristae and crista junctions in mitochondria depends on antagonism between Fcj1 and Su e/g. *J. Cell Biol.* **185**, 1047-1063.

Reers, M., Smiley, S. T., Mottola-Hartshorn, C., Chen, A., Lin, M. and Chen, L. B. (1995). Mitochondrial membrane potential monitored by JC-1 dye. *Methods Enzymol.* **260**, 406-417.

Rival, T., Soustelle, L., Cattaert, D., Strambi, C., Iché, M. and Birman, S. (2006). Physiological requirement for the glutamate transporter dEAAT1 at the adult Drosophila neuromuscular junction. *J. Neurobiol.* **66**, 1061-1074.

Rival, T., Macchi, M., Arnauné-Pelloquin, L., Poidevin, M., Maillet, F., Richard, F., Fatmi, A., Belenguer, P. and Royet, J. (2011). Inner-membrane proteins PMI/TMEM11 regulate mitochondrial morphogenesis independently of the DRP1/MFN fission/fusion pathways. *EMBO Rep.* **12**, 223-230.

Schleicher, M., Shepherd, B. R., Suarez, Y., Fernandez-Hernando, C., Yu, J., Pan, Y., Acevedo, L. M., Shadel, G. S. and Sessa, W. C. (2008). Prohibitin-1 maintains the angiogenic capacity of endothelial cells by regulating mitochondrial function and senescence. *J. Cell Biol.* **180**, 101-112.

Smiley, S. T., Reers, M., Mottola-Hartshorn, C., Lin, M., Chen, A., Smith, T. W., Steele, G. D., Jr and Chen, L. B. (1991). Intracellular heterogeneity in mitochondrial membrane potentials revealed by a J-aggregate-forming lipophilic cation JC-1. *Proc. Natl. Acad. Sci. USA* **88**, 3671-3675.

Strauss, M., Hofhaus, G., Schröder, R. R. and Kühlbrandt, W. (2008). Dimer ribbons of ATP synthase shape the inner mitochondrial membrane. *EMBO J.* **27**, 1154-1160.

Suen, D. F., Norris, K. L. and Youle, R. J. (2008). Mitochondrial dynamics and apoptosis. *Genes Dev.* **22**, 1577-1590.

Tanouye, M. A. and Wyman, R. J. (1980). Motor outputs of giant nerve fiber in Drosophila. *J. Neurophysiol.* **44**, 405-421.

Tondera, D., Grandemange, S., Jourdain, A., Karbowski, M., Mattenberger, Y., Herzig, S., Da Cruz, S., Clerc, P., Raschke, I., Merkwirth, C. et al. (2009). SLP-2 is required for stress-induced mitochondrial hyperfusion. *EMBO J.* **28**, 1589-1600.

Velours, J., Dautant, A., Salin, B., Sagot, I. and Brèthes, D. (2009). Mitochondrial F1F0-ATP synthase and organellar internal architecture. *Int. J. Biochem. Cell Biol.* **41**, 1783-1789.

Verstreken, P., Ly, C. V., Venken, K. J., Koh, T. W., Zhou, Y. and Bellen, H. J. (2005). Synaptic mitochondria are critical for mobilization of reserve pool vesicles at Drosophila neuromuscular junctions. *Neuron* **47**, 365-378.

Vogel, F., Bornhövd, C., Neupert, W. and Reichert, A. S. (2006). Dynamic subcompartmentalization of the mitochondrial inner membrane. *J. Cell Biol.* **175**, 237-247.

von der Malsburg, K., Müller, J. M., Bohnert, M., Oeljeklaus, S., Kwiatkowska, P., Becker, T., Loniewska-Lwowska, A., Wiese, S., Rao, S., Milenkovic, D. et al. (2011). Dual role of mitofilin in mitochondrial membrane organization and protein biogenesis. *Dev. Cell* **21**, 694-707.

Wakabayashi, J., Zhang, Z., Wakabayashi, N., Tamura, Y., Fukaya, M., Kensler, T. W., Iijima, M. and Sesaki, H. (2009). The dynamin-related GTPase Drp1 is required for embryonic and brain development in mice. *J. Cell Biol.* **186**, 805-816.

Westermann, B. (2010). Mitochondrial fusion and fission in cell life and death. *Nat. Rev. Mol. Cell Biol.* **11**, 872-884.

Wurm, C. A. and Jakobs, S. (2006). Differential protein distributions define two sub-compartments of the mitochondrial inner membrane in yeast. *FEBS Lett.* **580**, 5628-5634.

Xie, J., Marusich, M. F., Souda, P., Whitelegge, J. and Capaldi, R. A. (2007). The mitochondrial inner membrane protein mitofilin exists as a complex with SAM50, metaxins 1 and 2, coiled-coil-helix coiled-coil-helix domain-containing protein 3 and 6 and DnaJC11. *FEBS Lett.* **581**, 3545-3549.

Xu, Y., Condell, M., Plesken, H., Edelman-Novemsky, I., Ma, J., Ren, M. and Schlame, M. (2006). A Drosophila model of Barth syndrome. *Proc. Natl. Acad. Sci. USA* **103**, 11584-11588.

Zanna, C., Ghelli, A., Porcelli, A. M., Karbowski, M., Youle, R. J., Schimpf, S., Wissinger, B., Pinti, M., Cossarizza, A., Vidoni, S. et al. (2008). OPA1 mutations associated with dominant optic atrophy impair oxidative phosphorylation and mitochondrial fusion. *Brain* **131**, 352-367.

Zick, M., Rabl, R. and Reichert, A. S. (2009). Cristae formation-linking ultrastructure and function of mitochondria. *Biochim. Biophys. Acta* **1793**, 5-19.